ORIGINAL RESEARCH ARTICLE

Introduction of $Sr(In_{0.5}Ta_{0.5})O_3$ to Modulate Phase Structure and Optoelectronic Properties of $(K_{0.5}Na_{0.5})NbO_3$ Ceramics

Shaoyang Shi[1] · Gangbin Hu[1] · Mingchang Wang[1] · Huangtao Wu[1] · Xiang Liu[1] · Hua Wang[1,2] · Jiwen Xu[1,2] · Ling Yang[1] · Wei Qiu[1]

Abstract

Pressureless solid-phase sintering was used to prepare $(1-x)K_{0.5}Na_{0.5}NbO_3$-$xSr(In_{0.5}Ta_{0.5})O_3$ (KNN-xSInT, $x=0.02$, 0.03 0.04, 0.05, 0.06, 0.07) ceramics, and effects of SInT doping on the phase structure, microstructure, optical, and electrical properties in ceramics were investigated. With an increase in SInT content, the structure of KNN-xSInT ceramics gradually changes from orthogonal to pseudo-cubic . When $x=0.04$, the near-infrared band (1100 nm) transmittance of the ceramics reaches 46.92%, and the optical band gap (E_g) is 3.11 eV. The maximum dielectric constant (ε_r) is 4990 at $x=0.02$, and a maximum d_{33} value of 95 pC/N is obtained at $x=0.03$. The KNN-xSInT ceramic sample has characteristics of relaxation ferroelectrics, which is an environmentally friendly, lead-free transparent ferroelectric ceramic.

Keywords Transparent ceramics · phase structure · lead-free ceramics

Introduction

With the development of multifunctional ceramics, multifunctional ferroelectric ceramics with excellent ferroelectric, strain, energy storage, and other properties have become widely used in electronic components such as capacitors and transducers.[1] Transparent ferroelectric ceramics have excellent optoelectronic properties, which can combine physical quantities such as light, electricity, and mechanical deformation, allowing them to interact with each other, which results in promising applications within the fields of communications and integrated circuits.[2,3] (Pb, La)(Zr, Ti)O_3 (PLZT), as the typical representative of transparent ferroelectric ceramics, has various outstanding electro-optical effects, which have a wide range of applications in memory, optical switches, and displays.[4,5] For example, Zhang et al. exploited PLZT's large residual polarization intensity (P_r)

to enable its application for self-powered UV detectors and investigated the photoresponse performance of the detectors in detail.[6] Tang et al. proposed a photoelectric electrostatic compound-driven rotating micromirror using the anomalous photovoltaic effect of PLZT, which has a wide range of applications in medical imaging, communications and other fields.[7] However, the high lead (Pb) content of PLZT ceramics poses a risk to human health and the environment.[8] Therefore, the search for lead-free ceramics that can replace PLZT ceramics represents a promising research direction.

$(K_{0.5}Na_{0.5})NbO_3$ (KNN) ferroelectric ceramics possess a high Curie temperature (T_c) and a high piezoelectric coefficient (d_{33}),[9,10] making them the best alternative to lead-based ceramics.[11,12] However, KNN-based ceramics are typically not transparent,[13] and generally the transparency of ceramics is affected by multiple factors,[14,15] including crystal structure, grain boundary structure, grain size, porosity and impurities. By introducing a second phase, the phase structure of KNN-based ceramics shifts toward a highly symmetric pseudo-cubic phase, which improves the transparency of the ceramics.[10,16] Kwok et al. reported that Li and Bi co-doped $(K_{0.5}Na_{0.5})_{1-x}Li_xNb_{1-x}Bi_xO_3$ transparent ceramics were prepared by hot-pressure sintering, the light transmission of the ceramics reached 60% at 900 nm. The results show that the pseudo-cubic phase, the diffuse phase transition of the

✉ Hua Wang
  wh65@tom.com

[1] School of Materials Science and Engineering, Guilin University of Electronic Technology, Guilin 541004, People's Republic of China

[2] Guangxi Key Laboratory of Information Materials, Guilin University of Electronic Technology, Guilin 541004, People's Republic of China

ceramics, and the dense fine crystal structure are all responsible for the high transparency of the ceramics.[17]

In this study, SInT was introduced into the KNN matrix by a pressureless solid-phase sintering method. Replacing Na^+ (1.39 Å, CN = 12) with Sr^{2+} (1.44 Å, CN = 12), which has a slightly smaller ionic radius, and Nb^{5+} (0.64 Å, CN = 6) with In^{3+} (0.8 Å, CN = 6) and Ta^{5+} (0.64 Å, CN = 6), which has a slightly larger radius.[2,18,19] By ion substitution with slightly different radii, promising ceramic phase structure into highly symmetrical pseudo-cubic phase, producing ceramic samples with excellent optical and electrical properties. The effects of SInT content on the phase structure, microstructure, optical, dielectric, ferroelectric, and piezoelectric properties of the ceramics were also investigated.

Experimental Procedure

High-purity K_2CO_3 (99.5%), Na_2CO_3 (99.8%), Nb_2O_5 (99.99%), $SrCO_3$ (99.9%), and Ta_2O_5 (99.99%) as raw materials were used to prepare $(1-x)$ $(K_{0.5}Na_{0.5})$ NbO_3-xSr $(In_{0.5}Ta_{0.5})O_3$ (x = 0.02, 0.03 0.04, 0.05, 0.06, 0.07) ceramics by pressureless solid-phase sintering. Firstly, the raw materials were weighed according to the stoichiometric ratio, and were then ball-milled for 24 hours using anhydrous ethanol as ball milling medium. Secondly, the slurry was placed in a petri dish and dried in an oven at 70°C. The resulting powder was then placed in an alumina crucible and calcined at 860°C for 3 h, and the resulting calcined powder was subjected to a second ball milling for 12 h. Thirdly, the powder was mixed with a 7 wt.% polyvinyl alcohol (PVA) binder solution, ground and granulated, and passed through a 100 mesh screen. Finally, the powder was pressed into granules under a pressure of 5 MPa, and PVA was removed from the pellet by holding at 600°C, and then sintered at 1220°C for 3 h. The obtained ceramic sheets were polished to a thickness of 0.5 mm to test their optical properties, and silver electrodes were plated on the surface of the samples to test their electrical properties.

X-ray diffraction (XRD, D8 Advance, Bruker AXS) and field emission scanning electron microscopy (FE-SEM, Quanta 450 FEG, FEI) were used to test the phase structure and microscopic features of the samples. Optical transmittance of ceramics in the range of 300–1100 nm was measured with an ultraviolet–visible spectrophotometer (UV-6100, Metash, China). The hysteresis loops of the ceramics were tested at room temperature using a ferroelectric test system (P-PMF, Radiant). The dielectric properties were measured by a system consisting of a high-temperature test fixture, a high--temperature test rig, a dielectric test system software, and an impedance analyzer (4294A, Agilent) with a test temperature range of 0–500°C. The piezoelectric

constants (d_{33}, ZJ-3AN) were tested using a quasi-static d_{33} measuring instrument.

Results and Discussion

The XRD diffraction spectrum of KNN-xSInT (x = 0.02, 0.03, 0.04, 0.05, 0.06, 0.07) ceramics at room temperature and the XRD standard card of KNN ceramics (PDF#52–1583) are shown in Fig. 1a. Compared with the XRD standard card of KNN ceramics, all ceramic samples have a pure ABO_3 structure with no obvious second phase generation, indicating that SInT is well introduced into the KNN matrix to form a homogeneous solid solution. In addition, it is also found that there is a slight shift in the diffraction peak, which is caused by the addition of Sr^{2+} and In^{3+} ions into the KNN lattice.[11] In order to investigate the crystalline structure of the ceramics in detail, the (200) diffraction peak around 46° is enlarged locally as shown in Fig. 1b. At x = 0.02, the (200) diffraction peak splits into two peaks (002/020), and the intensity ratio between the two peaks is close to 2:1, indicating that the ceramic has an orthogonal phase structure.[19,20] As the content of SInT continues to increase, the two split diffraction peaks gradually merge into one sharp peak, and the phase structure of KNN-xSInT ceramics gradually transforms to pseudo-cubic phase.[21,22]

The lattice parameters (a, b, c), c/a ratio, and cell volume (V) of KNN-xSInT ceramics were calculated by the Jade 6.0 software, and the results are shown in Table I. When x = 0.02, the values of the lattice parameters (a, b, c) differ considerably and exhibit an orthogonal structure, which is corroborated by the XRD diffraction pattern in Fig. 1b. However, with the continued addition of SInT, the values of (a, b, c) gradually approach. In particular, the ratio of c/a gradually decreases, reaching a minimum value of 1.0037 at x = 0.04, at which point the symmetry of the ceramic is at its highest. In addition, with increase in SInT content, leading to more Sr^{2+} (1.44 Å, CN = 12) replacing Na^+ (1.39 Å, CN = 12), while In^{3+} (0.8 Å, CN = 6) and Ta^{5+} (0.64 Å, CN = 6) replaces Nb^{5+} (0.64 Å, CN = 6),[2,18,19] resulting in a distortion of the ceramic lattice, leading to a gradual increase in the cell size. As can also be seen in Fig. 1b, where the diffraction peaks are shifted to lower angles. It is worth noting that when $0.04 \leq x \leq 0.05$, (200) diffraction peak produces an abnormal phenomenon of moving to a high angle, which may be caused by defects.[12] Because of the different valence states of $(In_{0.5}Ta_{0.5})^{4+}$ and Nb^{5+}, oxygen vacancy defects will be generated inside the ceramics to maintain the total valence equilibrium during ion replacement. Oxygen vacancy presence will lead to the collapse and shrinking of the NbO_6 octahedra in the crystalline cell, thus making the crystalline cell smaller and shifting the diffraction peak to a high angle.[12,23]
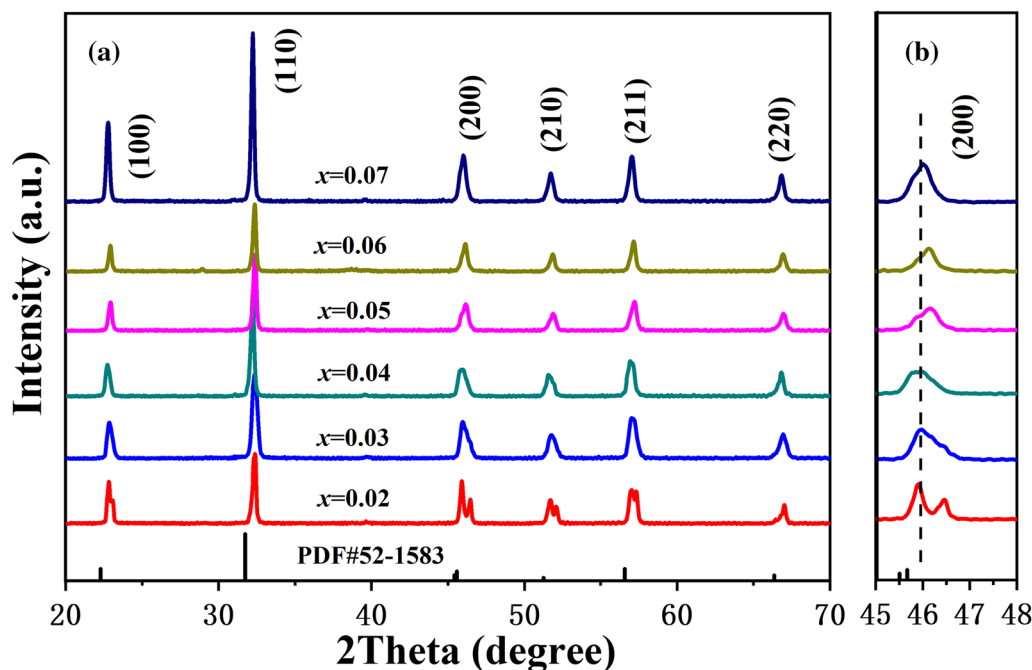
Fig. 1 (a) XRD patterns of KNN-xSInT ceramics and (b) expansions in the 2θ range at 45°–48°.

Table I Lattice parameters of KNN-xSInT ceramics

x	a	b	c	V (Å^3)	c/a
0.02	3.9056	3.9341	3.9774	61.11	1.0184
0.03	3.9404	3.9302	3.9660	61.42	1.0065
0.04	3.9442	3.9468	3.9590	61.63	1.0037
0.05	3.8855	3.9308	3.9495	60.32	1.0165
0.06	3.8816	3.9298	3.9518	60.28	1.0181
0.07	3.8825	3.9292	3.9602	60.41	1.0200

Densification and grain size play an extremely significant role in the transparency of ceramics.[24] Figure 2 shows the surface morphology of the KNN-xSInT ceramic samples with different SInT contents. As can be seen in Fig. 2, the ceramics show inhomogeneous grains and an arbitrary distribution of small and large grains. With increase in SInT content, the grain size of the ceramics gradually decreases overall, which indicates that the addition of SInT facilitates the grain refinement process. In addition, the microporosity of the ceramics shows an increase and enlargement. However, at $x = 0.04$, the grain size is evenly distributed and the micropores are small, leading to a reduction in light scattering and refraction processes. This is beneficial for obtaining high transmittance. When $x > 0.04$, the ceramic has an uneven distribution of grain size and numerous voids, which adversely affects its transparency. Thus, the ceramic exhibits a low transmittance.

From Fig. 3a, it can be seen that the texts beneath all the ceramic samples are visible, which indicates that the ceramic samples of all components have some light transmittance in the visible light band. To further investigate the effect of SInT content on transmittance, the transmittance analysis from the visible region (300 nm) to the near-infrared region (1100 nm) is performed in Fig. 3b. With the increase in SInT content, the transmittance of the ceramic increases and then decreases, reaching a maximum value of 46.92% in 1100 nm at $x = 0.04$. This is consistent with the results of the ceramic physical diagram. From Fig. 3b, it can be found that the transmittance of the ceramic is small and close to zero in the wavelength range from 300 to 400 nm, which is caused by the ceramic band gap jump.[19] By using the Tauc equation,[25] the optical band gap energy (E_g) of the ceramic is calculated. The equation is as follows:

$$(\alpha hv)^2 = A(hv - Eg) \tag{1}$$

where α and h are the absorption coefficient and Planck's constant, and v and A are photon frequency and constant. α can be calculated from the transmittance of the ceramic, and the equation is as follows:

$$\alpha = \frac{1}{t} \ln\left(\frac{1}{T}\right) \tag{2}$$

where t and T are the thickness and transmittance of the ceramic sample. The values of E_g can be obtained by extrapolating the slopes of the hv–$(ahv)^2$ scatter plot to 0, and the
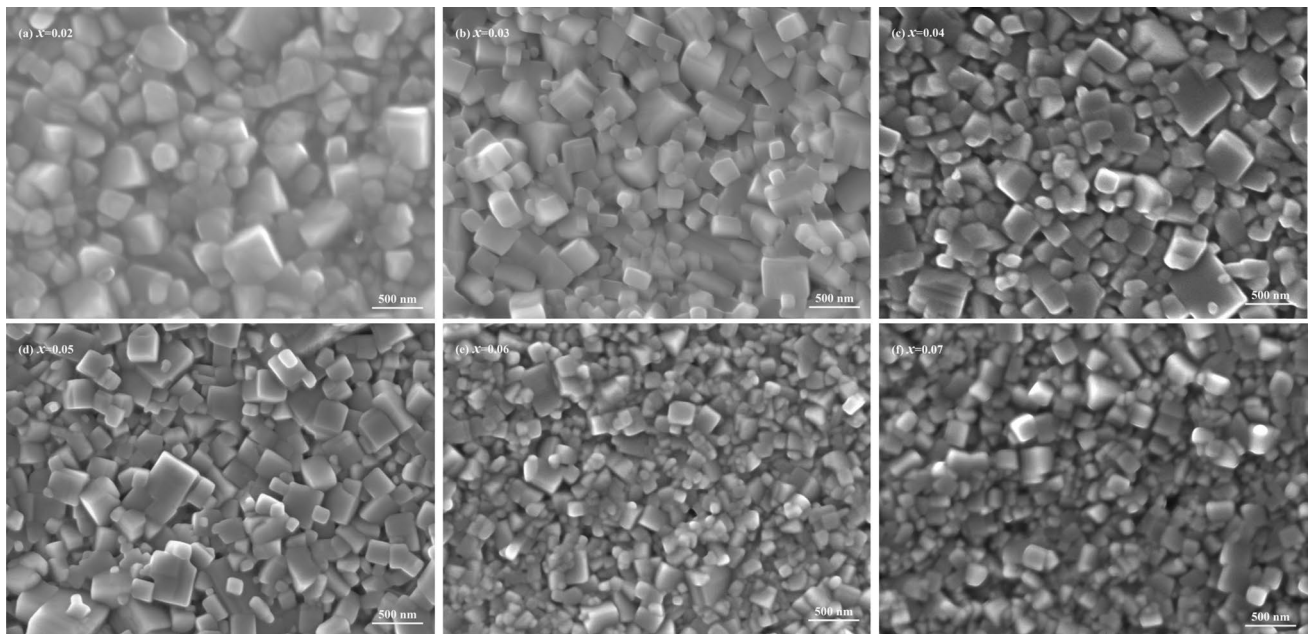
Fig. 2 KNN-*x*SInT ceramics surface morphology: (a) *x* = 0.02, (b) *x* = 0.03, (c) *x* = 0.04, (d) *x* = 0.05, (e) *x* = 0.06 and (f) *x* = 0.07.
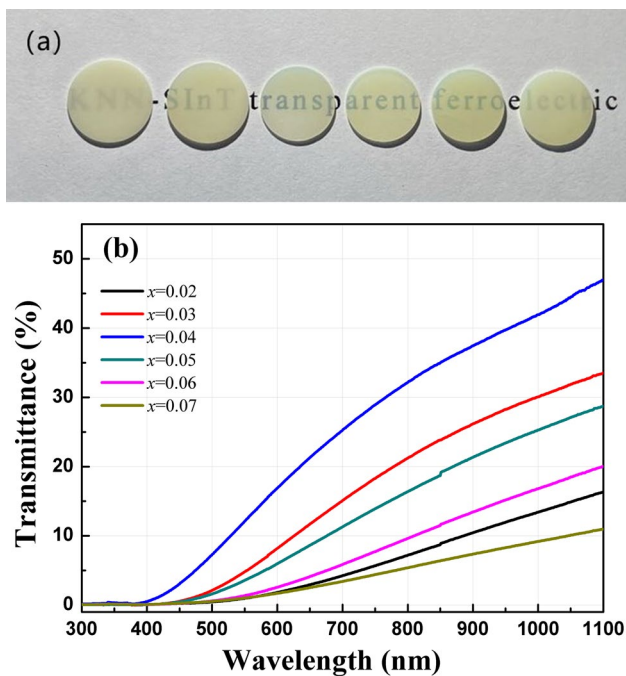
Fig. 3 (a) Photographs and (b) optical transmittance spectra of the KNN-*x*SInT ceramic.

results are shown in Fig. 4. It can be seen from Fig. 4 that E_g of all ceramic samples exceeds 2.65 eV. With increasing SInT content, E_g of ceramic samples shows a trend of increasing and then decreasing. At *x* = 0.04, E_g reaches a maximum value of 3.11 eV. The transmittance of ceramic

samples is closely related to the band gap energy. The energy of light can excite electrons from the valence band to the conduction band, during which some of the light is lost as electron jumping, and the remaining light is transmitted or scattered. If the forbidden bandwidth is large and the light source is not sufficient to cause an electron jump, the transmittance becomes high.[26]

Figure 5 shows the dielectric temperature spectra diagram of KNN-*x*SInT ceramics at temperatures from 0°C to 500°C. At *x* < 0.07, there are two anomalous peaks in the tested temperature range, corresponding to phase transitions from orthogonal to tetragonal and from tetragonal to cubic, respectively.[27] With increasing SInT content, the phase transition temperature range of the ceramics becomes progressively wider, indicating the presence of diffusive phase transition, which is typical for relaxed ferroelectrics.[28,29] It also shows that the introduction of SInT enhances the relaxation behavior of the ceramics.[10] When *x* = 0.07, the two dielectric peaks merge into one, indicating a change in the phase structure, which is consistent with the XRD test results. To investigate how the SInT content affects the dielectric properties of ceramics, Fig. 6a shows the dielectric temperature spectrum of KNN-*x*SInT ceramics at a frequency at 50 kHz. The Curie temperature (T_c) and the trend of the maximum dielectric constant (ε_r) with *x* are shown in Fig. 6b. The maximum permittivity decreased from 4990 at *x* = 0.02 to 1660 at *x* = 0.07, and the Curie temperature also decreased gradually from 367°C to 200°C. This is due to the transformation of the crystal structure to a more symmetrical
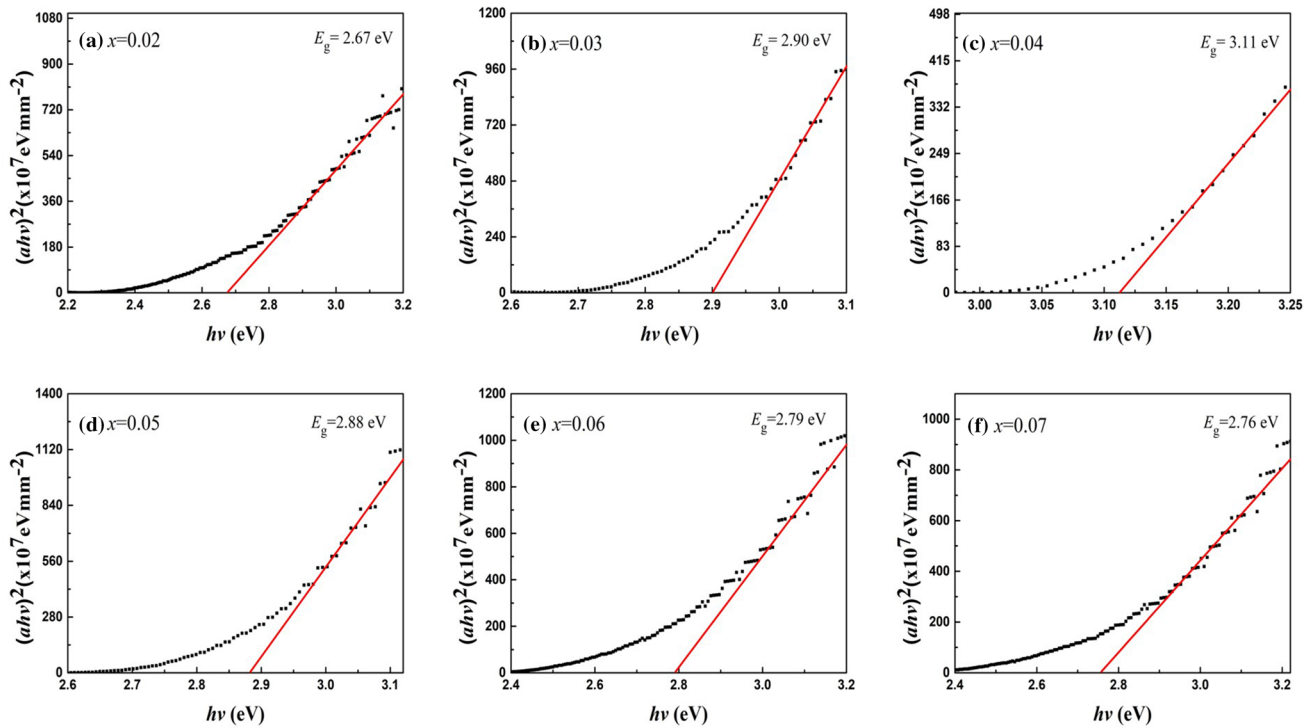
Fig. 4 Optical band gap diagrams of KNN-xSInT ceramics: (a) $x=0.02$, (b) $x=0.03$, (c) $x=0.04$, (d) $x=0.05$, (e) $x=0.06$ and (f) $x=0.07$.
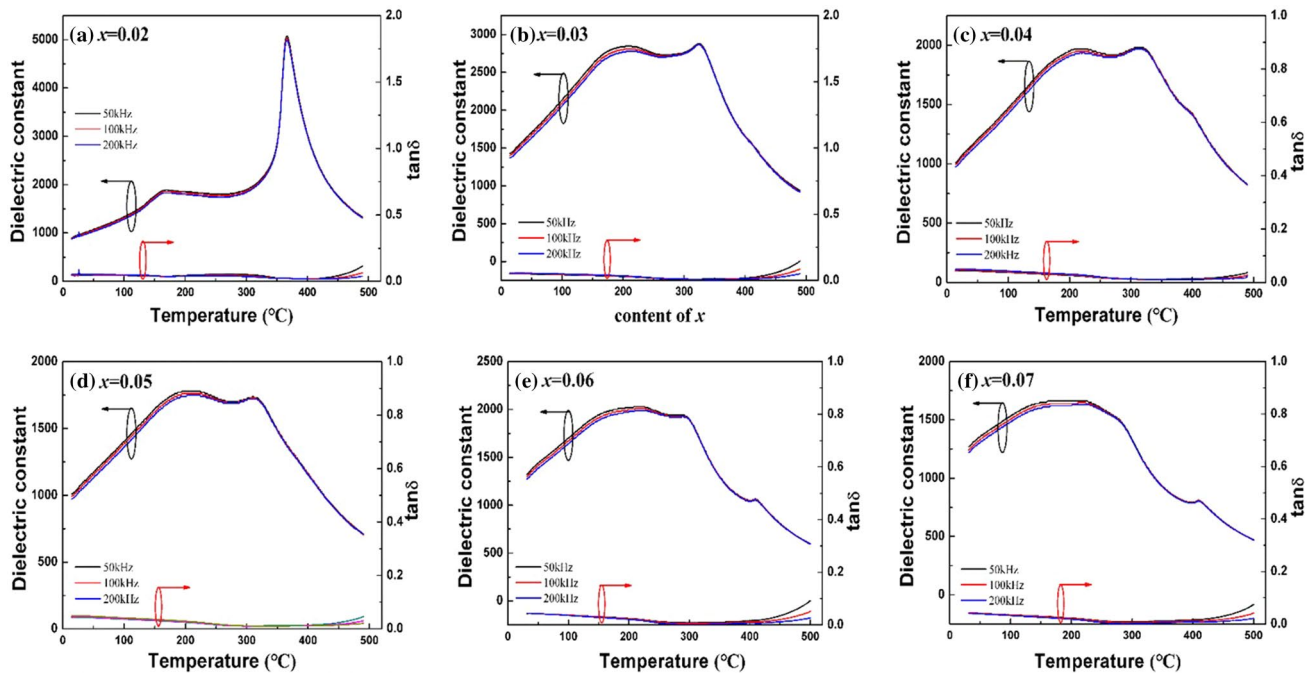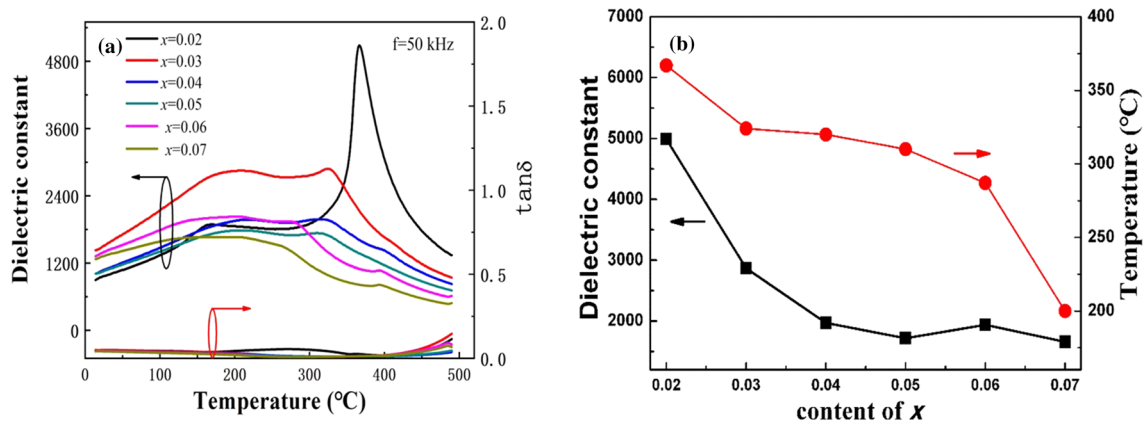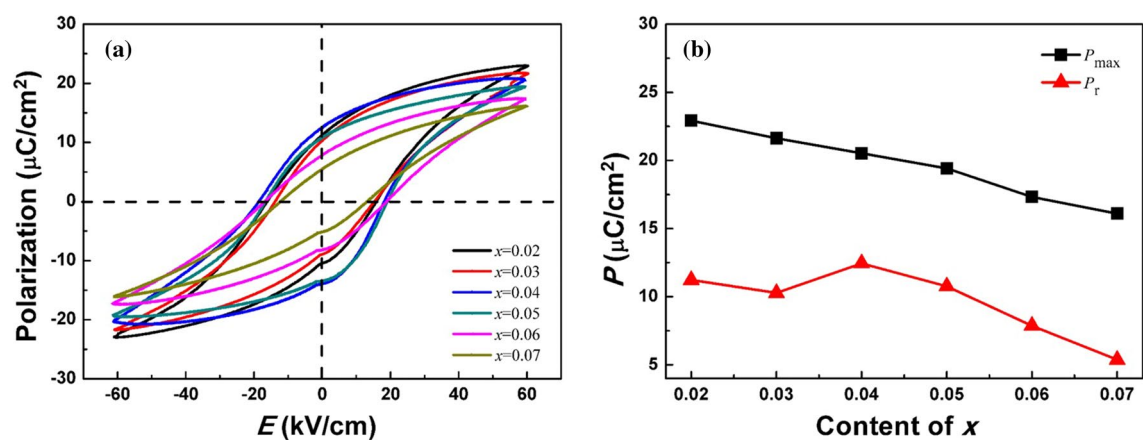

**Fig. 5** The dielectric temperature spectrum diagram of KNN-xSInT ceramics at temperatures from 0°C to 500°C.

Fig. 6 (a) The dielectric temperature spectrum diagram of KNN-xSInT ceramics at a frequency at 50 kHz. (b) Curie temperature (T_c) and the maximum dielectric constant variation curves.

Fig. 7 (a) The hysteresis lines (P–E) and (b) trend of P_m, P_r of the KNN-xSInT ceramic with an electric field of 60 kV/cm.

pseudo-cubic phase, which also reduces the ferroelectricity of the ceramics.

Figure 7a shows the hysteresis lines (P-E) of the KNN-xSInT ceramic sample under an electric field of 60 kV/cm. All ceramics show saturated and closed hysteresis lines, with the curves gradually changing from almost rectangular to almost linear, which further proves that the ceramics gradually become relaxed ferroelectrics.[30] The variation of saturation polarization intensity (P_m) and residual polarization intensity (P_r) in KNN-xSInT ceramic samples is given in Fig. 7b. It can be seen that with the increase in SInT content, P_m gradually decreases while P_r also presents a trend of gradual decrease, where the P_r value decreases from 11.2 μC/cm^2 at $x = 0.02$ to 5.4 μC/cm^2 at $x = 0.07$. This indicates that the ferroelectric properties in ceramics are weakened due to the progressive enhancement of relaxation behavior.[31]
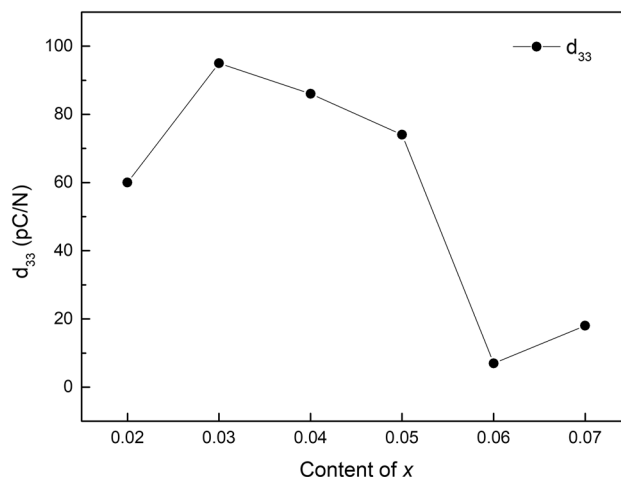
Fig. 8 The value of the piezoelectric coefficient (d_{33}) for KNN-xSInT ceramics.

Figure 8 shows the value of the piezoelectric coefficient (d_{33}) for KNN-xSInT ceramics. With the addition of SInT, the d_{33} value tends to increase rapidly and then decrease gradually, indicating that a small amount of SInT is added to facilitate the increase of the piezoelectric coefficient. A maximum d_{33} value of 95 pC/N is obtained at $x = 0.03$. This value is slightly lower than the d_{33} value for pure KNN, which is 115 pC/N.[32] Although the value of d_{33} is slightly reduced, the ceramic still obtains a high Curie temperature. The favorable optoelectronic properties and the high Curie temperature indicate the potential application of this ceramic in the field of multifunctional optoelectronic devices over a wide temperature range.

Conclusions

In this experiment, KNN-xSInT transparent ferroelectric ceramics were synthesized by the pressureless solid-phase sintering method. With increasing SInT content, the phase structure gradually changes from an orthogonal phase to pseudo-cubic phase. The symmetry of the ceramics is improved and the light transmission is enhanced. At $x = 0.04$, the ceramic transmittance reaches a maximum of 46.92% at 1100 nm, while the optical band gap reaches a maximum of 3.11 eV. When $x > 0.04$, a large grain size and voids are present at the grain boundaries, which has a negative effect on the transparency of the ceramic. In addition, the incorporation of SInT enhances crystallographic symmetry, leading to a weakening of the electrical properties of the ceramics. With increase in SInT content, the maximum dielectric constant and P_r in ceramic samples shows a decreasing trend. The maximum dielectric constant decreases from 4990 to 1660, and P_r decreases from 11.2 μC/cm^2 to 5.4 μC/cm^2. A maximum d_{33} value of 95 pC/N is obtained at $x = 0.03$. Furthermore, the ceramic samples exhibit the characteristics of relaxation ferroelectrics. Compared with single crystal materials and lead-based transparent ferroelectric ceramics, the preparation process is simple, low cost, and suitable for mass production. Therefore, KNN-based ceramics have more practical and broad application prospects in the field of optoelectronic devices.

References

1. Y. Sun, H. Wang, G. Liu, H. Xie, C. Zhou, G. Chen, C. Yuan, and X. Jiwen, High Energy Storage Efficiency and High Electrostrictive Coefficients in BNT–BS–xBT Ferroelectric Ceramics. *J. Mater. Sci. Mater. Electron.* 31, 5546 (2020).

2. X.M. Zhao, X.L. Chao, D. Wu, P.F. Liang, and Z.P. Yang, Evaluation of Birefringence Contribution to Transparency in (1–x)KNN-xSr(Al0.5Ta0.5)O3 Ceramics: A Phase Structure Tailoring. *J. Alloys Compd.* 798, 669 (2019).

3. S.F. Wang, J. Zhang, D.W. Luo, F. Gu, D.Y. Tang, Z.L. Dong, G.E.B. Tan, W.X. Que, T.S. Zhang, S. Li, and L.B. Kong, Transparent Ceramics: Processing, Materials and Applications. *Prog. Solid State Chem.* 41, 20 (2013).

4. J.J. Zhang, X.D. Su, M.R. Shen, Z.H. Dai, L.J. Zhang, X.Y. He, W.X. Cheng, M.Y. Cao, and G.F. Zou, Enlarging Photovoltaic Effect: combInation of Classic Photoelectric and Ferroelectric Photovoltaic Effects. *Sci Rep.* 3, 2109 (2013).

5. Y.J. Tang, Y.S. Chen, K. Qiao, and X.J. Wang, Micro-Mirror with Hybrid Photoelectric-Electrostatic Driving of PLZT Ceramic. *IOP Conf. Ser. Mater. Sci. Eng.* 307, 012016 (2018).

6. Y. Zhang, J. Chen, Q.F. Zhang, Y.M. Lu, H.T. Huang, and Y.B. He, Ultrasensitive Self-Powered UV PDs Via Depolarization and Heterojunction Fields Jointly Enhanced Carriers Separation. *J. Am. Ceram. Soc.* 104, 928–935 (2020).

7. Y.J. Tang, Z. Yang, Y.S. Chen, and X.J. Wang, PLZT Ceramic Driving Rotary Micro-mirror Based on Photoelectric-electrostatic Mechanism. *IOP Conf. Ser. Mater. Sci. Eng.* 275, 012048 (2017).

8. P.K. Panda, Review: Environmental Friendly Lead-Free Piezoelectric Materials. *J. Mater. Sci.* 44, 5049–5062 (2009).

9. H. Wang, X. Zhai, J.W. Xu and L. Yang, Effect of Sintering Time on Structure and Properties in CuO-doping KNN-LS-BF Piezoelectric Ceramics. *J. Wuhan Univ. Technol Mater. Sci. Ed.* 34, 308–311 (2019).

10. M. Zhang, H. Yang, D. Li, and Y. Lin, Excellent Energy Density and Power Density Achieved in K$_{0.5}$Na$_{0.5}$NbO$_3$-Based Ceramics with High Optical Transparency. *J. Alloys Compd.* 829, 154565 (2020).

11. H.N. Liu, J.T. Wang, H. Wang, J.W. Xu, C.R. Zhou, and W. Qiu, Er^{3+} and Sr(Bi$_{0.5}$Nb$_{0.5}$)O$_3$-Modified (K$_{0.5}$Na$_{0.5}$)NbO$_3$: A New Transparent Fluorescent Ferroelectric Ceramic with High Light Transmittance and Good Luminescence Performance. *Ceram. Int.* 48, 4230 (2022).

12. H.T. Wu, G.B. Hu, S.Y. Shi, X. Liu, H. Wang, J.W. Xu, L. Yang, W. Qiu, and S.J. Zhou, Effect of Ho Addition on the Optical and Electrical Properties of 0.98KNN-0.02SYT Ceramics. *J. Electron. Mater.* 51, 831 (2021).

13. H. Wang, X.Y. Zhao, J.W. Xu, X. Zhai, and L. Yang, Revised Effective Ionic Radii and Systematic Studies of Interatomie Distances in Halides and Chaleogenides. *Bull. Mater. Sci.* 39, 743 (2016).

14. A.R. Boccaccini and D.D. Silva, Industrial Developments in the Field of Optically Transparent Inorganic Materials: A Survey of Recent Patents. *Recent Pat. Mater. Sci.* 1, 56 (2008).

15. G.B. Hu, H.N. Liu, J.T. Wang, Y.B. Sun, H. Wang, J.W. Xu, L. Yang, and C.R. Zhou, Regulating the Structural, Transmittance, Ferroelectric, and Energy Storage Properties of K$_{0.5}$Na$_{0.5}$NbO$_3$ Ceramics Using Sr(Yb$_0$.5Nb0.5)O$_3$. *J. Electron. Mater.* 50, 968 (2020).

16. L. Zhang, Y.P. Pu, M. Chen, T.C. Wei, W. Keipper, R.K. Shi, X. Guo, R. Li, and X. Peng, High Energy-Storage Density Under

Low Electric Fields and Improved Optical Transparency in Novel Sodium Bismuth Titanate-based Lead-Free Ceramics. *J. Eur. Ceram. Soc.* 40, 71 (2020).

17. F.L. Li and K.W. Kwok, Fabrication of transparent electro-optic $(K_{0.5}Na_{0.5})_{1-x}Li_xNb_{1-x}Bi_xO_3$ lead-free ceramics. *J. Eur. Ceram. Soc.* 33, 123 (2013).

18. R.D. Shannon, Revised Effective Ionic Radii and Systematic Studies of Interatomie Distances in Halides and Chaleogenides. *Acta Cryst.* 32, 751 (1976).

19. H. Xie, G.B. Liu, L. Yang, S.J. Pang, C.L. Yuan, X.W. Zhang, H. Wang, C.R. Zhou, and J.W. Xu, Excellent Optical, Dielectric, and Ferroelectric Properties of $Sr(In_{0.5}Nb_{0.5})O_3$ Modified $K_{0.5}Na_{0.5}NbO_3$ Lead-Free Transparent Ceramics. *J. Mater. Sci. Mater. Electron.* 29, 19123 (2018).

20. X.D. Ren, Q.Z. Chai, X.M. Zhao, Z.H. Peng, D. Wu, P.F. Liang, L.L. Wei, Z.P. Yang, and X.L. Chao, Relaxor Behaviors and Electric Response in Transparent $0.95(K0.5Na0.5NbO3)0.05Ca(ZrxZnyNbz)1.025O3$ Ceramics with Low-Symmetric Structure. *Ceram. Int.* 45, 3961 (2019).

21. Y.J. Zhao, J.L. Liu, X.W. Zhang, and H.P. Zhou, Domain Switching Mechanism of Orthorhombic-Tetragonal Coexistence (Li, K, Na)N_bO3 Ceramics. *J. Alloys Compd.* 763, 695 (2018).

22. Y.J. Zhao, J.L. Liu, and D. Yan, Improved Piezoelectric and Strain Performance of $Na_2B_4O_7$-Doped (Li, K, Na)N_bO3 lead-free piezoceramics. *J. Mater. Sci.* 54, 1126 (2018).

23. M.Q. Awan, J. Ahmad, A. Berlie, Q.B. Sun, R.L. Withers, and Y. Liu, The Upper Manganese Doping Limit and its Effects on Physical Properties of Lead-Free $Bi_{0.5}Na_{0.5}TiO_3$ Ceramics. *Ceram. Int.* 44, 12767 (2018).

24. Y.Y. Liu, Y.H. Yi, Y.G. Yu, Y.Q. Pan, C.W. He, X.K. Liu, Z.P. Xu, G. Liu, and Y. Chen, Microstructures, Phase Evolution and Electrical Properties of (1–x) $K0.40Na0.60Nb0.96Sb0.04O3$-$xBi0.5K0.5HfO3$ Lead-Free Ceramics. *Ceram. Int.* 45, 6328 (2019).

25. C. Lin, X. Wu, M. Lin, Y.P. Huang, and J. Li, Optical, luminescent and Optical Temperature Sensing Properties of $(K_{0.5}Na_{0.5})NbO_3$-$ErBiO_3$ Transparent Ceramics. *J. Alloys Compd.* 706, 156 (2017).

26. J.F. Lin, Q.L. Lu, J. Xu, X. Wu, C. Lin, T.F. Lin, C. Chen, and L.H. Luo, Outstanding Optical Temperature Sensitivity and Dual-Mode Temperature-Dependent Photoluminescence in Ho^{3+}-Doped (K, Na)Nb_O3–$SrTi_O3$ Transparent Ceramics. *J. Am. Ceram. Soc.* 102, 4710 (2019).

27. D. Yang, Z.Y. Yang, X.S. Zhang, L.L. Wei, X.L. Chao, and Z.P. Yang, High Transmittance in Lead-Free Lanthanum Modified Potassium-Sodium Niobate Ceramics. *J. Am. Ceram. Soc.* 716, 21 (2017).

28. X.H. Ren, Z.H. Peng, B. Chen, Q.Q. Shi, X.S. Qiao, D. Wu, G.R. Li, L. Jin, Z.P. Yang, and X.L. Chao, A Compromise Between Piezoelectricity and Transparency in KNN-Based Ceramics: The Dual Functions of Li_2O Addition. *J. Eur. Ceram. Soc.* 40, 2331 (2020).

29. B.Y. Qu, H.L. Du, and Z.Y. Yang, Lead-Free Relaxor Ferroelectric Ceramics with High Optical Transparency and Energy Storage Ability. *J. Mater. Chem. C.* 4, 1795 (2016).

30. A. Chitra, R. Khandelwal, R. Laishram. Gupta, and K.C. Singh, Impact of Crystal Structure and Microstructure on Electrical Properties of Ho Doped Lead-Free BCST Piezoceramics. *Ceram. Int.* 45, 10371 (2019).

31. X.S. Zhang, D. Yang, Z.Y. Yang, X.M. Zhao, Q.Z. Chai, X.L. Chao, L.L. Wei, and Z.P. Yang, Transparency of $K_{0.5}N_{0.5}NbO_3$-$Sr(Mg_{1/3}Nb_{2/3})O_3$ Lead-Free Ceramics Modulated by Relaxor Behavior and Grain Size. *Ceram. Int.* 42, 17963 (2016).

32. X.Y. Sun, J. Chen, R.B. Yu, C. Sun, G.R. Liu, X.R. Xing, and L.J. Qiao, $BiScO_3$ Doped $(Na_{0.5}K_{0.5})NbO_3$ Lead-Free Piezoelectric Ceramics. *J. Am. Ceram. Soc.* 92, 130 (2009).